Characterization of Orsay virus replication intermediates in *Caenorhabditis elegans* reveals links to antiviral RNA interference

Supraja Ranganathan, P. Joseph Aruscavage, Brenda L. Bass

Department of Biochemistry, University of Utah, Salt Lake City, Utah, USA 84112-5650

Running title: Viral replication intermediates and RNAi

Abbreviations:

RNA – Ribonucleic acid

DNA – Deoxyribonucleic acid

OV – Orsay Virus

RdRP – RNA-dependent RNA Polymerase

RNAi – RNA interference

dsRNA – double stranded RNA

siRNA - small interfering RNA

+ssRNA – positive, single strand RNA

OVIGs – OV induced genes

AVC – Antiviral complex

hpi – hours post infection

PCR – Polymerase Chain Reaction

RT-qPCR – Reverse transcription quantitative PCR

smFISH – single molecule fluorescence in-situ hybridization

dsmFISH – denature smFISH

GFP – Green Fluorescent Protein

NGM – Nematode Growth Medium

PBS – Phosphate buffer saline

RT – room temperature

ANOVA – analysis of variance

Abstract

Orsay Virus (OV) is a positive-sense, single-stranded RNA (+ssRNA) virus that naturally infects *C. elegans* intestines. Like other +ssRNA viruses, the OV-encoded RNA-dependent RNA polymerase (oRdRP) synthesizes complementary antigenome for use as template for amplifying viral genome, but OV replication intermediates are underexplored. Using PCR, we observed viral genome in vast excess of antigenome, as for other +ssRNA viruses. Unlike interferon-based antiviral defense, *C. elegans* utilizes RNA interference (RNAi) for antiviral defense, producing sense and antisense small interfering RNAs (siRNAs) that cannot be distinguished from genome and antigenome with conventional hybridization protocols. Fluorescence-based imaging in *C. elegans* intestines using probes to antigenomic sequences revealed cytoplasmic as well as perinuclear localization patterns. The latter depended on factors required for generation of primary, but not secondary, siRNAs, connecting the antigenomic hybridization pattern to RNAi. We also observed cytoplasmic double-stranded RNA (dsRNA) associated with oRdRP, suggesting viral replication hubs, as well as infection-induced nuclear dsRNA, likely from endogenous dsRNA. Finally, using antibodies to oRdRP, we observed spherical structures of ~1μm in diameter with oRdRP at their surface, which decrease in animals lacking RDE-1. Our study defines features of OV replication intermediates, setting the stage for understanding their connection to host antiviral pathways.

44 **Significance Statement:**

45 - Orsay virus is a +ssRNA virus that infects *C. elegans* intestines. We advance understanding of
46 viral replication intermediates and address the issue that for animals that use antiviral RNA
47 interference, hybridization of probes occurs with both genome and antigenome and small
48 interfering RNAs.
49 - Single-molecule fluorescence in-situ hybridization using antigenomic probes revealed
50 cytoplasmic and perinuclear puncta, only upon denaturation, with perinuclear signal dependent
51 on primary, but not secondary, siRNA biogenesis. Viral RNA-dependent RNA polymerase lined
52 the perimeter of spherical structures of ~1μm diameter.
53 - This study sets the stage for understanding the relationship between viral replication dynamics
54 and antiviral RNA interference.

55 **Introduction**

56 Orsay Virus (OV) is a naturally infecting *C. elegans* pathogen that closely resembles the
57 *Nodaviridae* family of viruses. OV is a positive strand, single-stranded RNA (+ssRNA) virus, with a
58 bipartite genome (oRNA1 and oRNA2), that preferentially infects *C. elegans* intestinal cells where it is
59 predominantly restricted to anterior cells (Félix *et al.*, 2011; Franz *et al.*, 2014; Castiglioni *et al.*, 2024).
60 oRNA1 encodes an RNA-dependent RNA Polymerase (oRdRP), and oRNA2 encodes the capsid,
61 δ (delta), and capsid-δ fusion proteins (Félix and Wang, 2019).

62 While details of OV replication and its intermediates are just emerging (Franz *et al.*, 2014;
63 Batachari *et al.*, 2024), it can be presumed that general features of positive-strand RNA viruses are
64 operative (de Beijer *et al.*, 2024; Stancheva and Sanyal, 2024). Replication of a positive-strand RNA
65 virus begins with translation of its RdRP from the genomic strand. The RdRP first synthesizes a
66 complementary strand to the genome, the antigenome (-ssRNA), and this is the first RNA replication
67 intermediate. The antigenome is then used as a template by the RdRP to amplify the viral genome
68 (Ball, 1994). The perfectly complementary strands of genome and antigenome can basepair to form a
69 viral double-stranded RNA (dsRNA), another RNA intermediate of viral replication. Replication of
70 closely related nodaviruses occurs inside membrane-enclosed compartments that protect viral RNA
71 and other replication intermediates from the host antiviral machinery (Stancheva and Sanyal, 2024).
72 The structural proteins along with the viral genome they encapsulate are packaged and processed into
73 a mature virion that is then egressed out of the cell.

74 Some viral replication intermediates are recognized by helicases to elicit an antiviral response.
75 Among vertebrates, the RIG-I-like Receptor (RLR) family of helicases recognize dsRNA to elicit an
76 interferon response. Invertebrates do not have interferon pathways, and invertebrates such as *C.*
77 *elegans* instead utilize RNA interference (RNAi). In RNAi it is the enzyme Dicer that recognizes dsRNA,
78 using a helicase domain related to that of RLRs. *C. elegans* Dicer (DCR-1) forms an antiviral RNAi
79 complex with DRH-1, a Dicer-related helicase and RLR ortholog, and RDE-4 (RNAi-DEficient 4), a
80 dsRNA binding protein. This antiviral complex (AVC) cleaves viral dsRNA into 23H (H=A,U,C>G at 5'
81 end) primary small-interfering RNAs (1° siRNAs). The 1° siRNA is then bound by RDE-1 (RNAi-

82 deficient 1), an argonaute protein, and passed to other factors for generation and amplification of 22G
83 (preferentially G at 5' end) secondary siRNAs (2° siRNAs) that are complementary to the viral genome
84 (Ashe *et al.*, 2013; Guo *et al.*, 2013). In the germline, amplification of 2° siRNAs occurs in perinuclear
85 compartments that are marked by the presence of RNAi amplification factors such as RRF-1 and DRH-
86 3 (Phillips *et al.*, 2012). However, very little is known about the spatial organization of RNAi factors and
87 RNAi hubs in somatic tissues, such as the intestine, and during OV infection.

88 Somewhat analogous to the mammalian interferon response, the *C. elegans* antiviral response
89 also involves transcription of OV-induced genes (OVIGs) (Chen *et al.*, 2017; Castiglioni *et al.*, 2024), a
90 subset of which are the *C. elegans* Intracellular Pathogen Response (IPR) genes (Reddy *et al.*, 2017);
91 transcription of OVIGs requires DRH-1, but not DCR-1 or RDE-4 (Sowa *et al.*, 2019). DRH-1-mediated
92 OVIG induction occurs after viral replication, but the exact viral intermediate that DRH-1 recognizes to
93 trigger OVIGs is unknown. However, recently OV dsRNA was visualized in association with DRH-1 in *C.*
94 *elegans* intestines, raising the possibility that this recognition is important for triggering OVIGs
95 (Batachari *et al.*, 2024). *C. elegans* lacking RNAi factors have increased sensitivity to OV, and these
96 mutant strains are widely used to understand OV replication dynamics and downstream RNAi
97 responses (Franz *et al.*, 2014). Given that replication is required to elicit host antiviral responses, it is
98 important to understand the temporal and spatial organization of replication intermediates. The most
99 well-studied viral replication byproduct is viral dsRNA. We know less about other replication
100 intermediates, leading to an incomplete picture of replication dynamics and antiviral responses, and for
101 *C. elegans*, this is especially true for a wildtype background.

102 Here we describe studies designed to detect and characterize three replication intermediates,
103 oRNA1 antigenome, OV dsRNA, and oRdRP, in both wildtype and RNAi mutant backgrounds. We show
104 that OV is like other +ssRNA viruses in that the viral genome is present in vast abundance relative to
105 the antigenome, in both wildtype and RNAi mutants. Single molecule FISH (smFISH) using probes
106 designed to detect antigenomic sequences show signal in cells with genomic strand, and detection is
107 facilitated with denaturation protocols, indicating most antigenomic sequences are basepaired. Apart
108 from the expected cytoplasmic distribution, unexpectedly, we observed signal with antigenomic probes

109 within perinuclear regions; fewer animals showed this signal in strains defective for primary siRNA
110 biogenesis, but not those aberrant for secondary siRNA amplification, setting the stage for connecting
111 OV infection and replication with the antiviral RNAi pathway. We did not detect RNAi factors associating
112 with the perinuclear-localized antigenomic signal, unlike *C. elegans* germline. We observed oRdRP-
113 associated dsRNA puncta revealing possible replication hubs. Infected wildtype intestinal cells also
114 showed oRdRP in lumen-containing spherical structures of ~1μm in diameter that were dependent on
115 factors of the antiviral RNAi pathway. Together, the results reveal new hubs of viral replication and
116 processing, specifically in a wildtype background.

117 **Results**

118 **OV genomic strand accumulates significantly more than antigenomic strand in wildtype and**
119 **RNAi mutants**

120 OV infection in *C. elegans* is typically measured by RT-qPCR in a strand-agnostic manner and
121 denoted as viral load, or by monitoring genomic strand accumulation using northern blot analysis. For a
122 plus-strand virus such as OV, these methods largely reflect levels of the more abundant genome but
123 offer little information about the less abundant antigenome (Félix *et al.*, 2011). To acquire this
124 information, we first monitored OV-infected animals with strand-specific RT-qPCR. We designed strand-
125 specific probes for oRNA1 genome or antigenome that each included a unique flanking sequence so
126 that strand-specific complementary DNA (cDNA) could be quantified with qPCR, using the unique
127 flanking region as a primer and a second downstream on the respective oRNA1 strand (**Figure 1A**).
128 We also performed northern blot analysis to complement our strand-specific RT-qPCR method and
129 directly detect viral RNA abundance.

130 We in vitro transcribed and purified fragments of genomic and antigenomic strands of oRNA1,
131 each ~500 nucleotides (nts) long, and used these transcripts to generate standard curves for
132 quantifying copy number in a strand-specific manner (**Supplemental Figures 1A and 1B**); these
133 transcripts were also used to confirm that antigenomic probes were specific and able to detect 10^6
134 copies of purified ~500nt antigenome ssRNA by northern blot assay (**Supplemental Figure 1C)**. We
135 then monitored appearance of genome and antigenome over time, using two infection protocols: one

136 monitoring infection of L3 larvae at 12- and 24-hours post infection (hpi; **Figure 1B**), and a second
137 aimed at quantifying strands after prolonged infection, by infecting L1 larvae and assaying 48 and 72hpi
138 (**Figure 1C**). For the latter, we chose infection times that maintained animals in the same reproductive
139 cycle (72hpi) so that populations would not be contaminated with newly hatched larvae.

140 For each protocol, we compared infection of wildtype (N2) animals to that observed in antiviral
141 RNAi mutants, *drh-1(uu60), rde-4(uu71), rde-1(ne219)*, and a helicase point mutant (G492R*)* of DCR-1
142 (*eri-4(mg375)*) (Pavelec *et al.*, 2009a; Welker *et al.*, 2010), referred to here as *dcr-1(mg375)* (**Figures**
143 **1D and 1E**). We observed significantly higher levels of genome than antigenome for wildtype and RNAi
144 mutant strains. Further, for each infection protocol, with few exceptions, we observed a dramatic and
145 significant increase in oRNA1 genome copy numbers at 24hpi and 72hpi relative to 12hpi or 48hpi,
146 respectively, in both wildtype and mutant animals. We observed a modest increase in oRNA1
147 antigenome relative to wildtype in *drh-1, rde-4* or *rde-1* mutants, but at early time points this was not
148 observed in *dcr-1(mg375)* mutants (**Figures 1D and 1E; points relative to pink dotted line**).
149 Quantification showed greater than 100-fold increase in genome over antigenome at 12hpi, and over
150 1000-fold increase at all other infection times, for both wildtype and RNAi mutants (**Supplemental**
151 **Figures 1D and 1E**). Northern blot analyses confirmed the low levels of antigenome compared to
152 genome (**Supplemental Figures 1F and 1G**); controls established that if present antigenome could be
153 detected, but oRNA1 antigenome was below the limit of detection for wildtype and RNAi mutants at all
154 time points tested (12-72 hpi). oRNA1 genome was first detected at 24hpi for RNAi mutants, and
155 increased over time, but was only faintly detected at 72hpi for wildtype strains.

156 Consistently, levels of genomic RNA were higher in RNAi mutants than wildtype (**Figures 1D**
157 **and 1E**), and trends matched the increase in viral load as determined in a strand-agnostic manner,
158 consistent with prior studies (Ashe *et al.*, 2013; Sowa *et al.*, 2019) (**Supplemental Figures 1H and 1I).**
159 In accordance with published studies, we observed that the antiviral RNAi mutants, *drh-1*, *rde-4* and
160 *rde-1*, were sensitive to OV and showed increased viral load relative to wildtype at all timepoints tested,
161 by all methods (Ashe *et al.*, 2013). While previous studies have reported the sensitivity of *dcr-1* using
162 deletion mutants or knockdown (RNAi) (Ashe *et al.*, 2013; Sowa *et al.*, 2019), we report the involvement

163 of the helicase domain of DCR-1. The helicase mutant *dcr-1(mg375)* showed a delayed response with
164 a moderate increase in viral load, ~10-fold at 12hpi and 24hpi, and ~100-fold at 48hpi and 72hpi
165 **(Figures 1D and 1E; Supplemental Figures 1H and 1I)**.
166 Prior studies have looked at viral infection in the constitutively infected JU1580 strain, which has
167 a mutation in DRH-1 and is highly sensitive to OV infection (Félix *et al.*, 2011; Félix and Wang, 2019).
168 To connect our studies to prior studies we showed that a high viral load in the JU1580 strain relative to
169 wildtype, as determined using strand-agnostic protocols, correlated with a robust accumulation of
170 oRNA1 genomic strand by both strand-specific RT-qPCR and northern blot, while the oRNA1
171 antigenome levels remained significantly lower, ~1300-fold, (*p-value<0.0001*) (**Figures 1F;**
172 **Supplemental Figures 1F and 1G**). This emphasizes that the antigenomic strand is much lower than
173 the genomic strand even with constitutive infection. To test if the ratio of genome to antigenome was a
174 property inherent to oRdRP mediated replication, we also monitored a heat shock-inducible replicon
175 system expressing wildtype ($oRdRP^{WT}$) or a replication-incompetent mutant ($oRdRP^{mut}$) oRNA1 (Jiang
176 *et al.*, 2017). In the complete absence of infection, we observed a significant increase in genome and
177 antigenome upon inducing the expression of $oRdRP^{WT}$ but not $oRdRP^{mut}$, and notably, antigenome
178 levels remained significantly lower (**Figure 1G**), which was confirmed by northern blot (**Supplemental**
179 **Figure 1F**).
180 In summary, these studies indicate that the increase in viral load commonly measured using
181 strand-agnostic methods largely reflects an increase in genomic strand. At the time points tested, for
182 wildtype and RNAi mutant strains, we found that the genomic strand, the strand that is packaged into
183 virions, is in far excess of the antigenomic strand, which is only an intermediate, and these ratios are
184 intrinsic to the oRdRP and its tight regulation by host factors (Ahlquist *et al.*, 2003; Jakubiec and Jupin,
185 2007).
186 **Signal using probes to the oRNA1 antigenome is present upon denaturation**
187 To gain insight into the localization of OV genome and antigenome within infected cells, we
188 performed smFISH analyses by designing multiple strand-specific fluorescent deoxyoligonucleotide
189 probes for oRNA1 (27 probes, genomic strand; 48 probes, antigenomic strand). For initial optimization,

190 we used OV infection-sensitive *jyIs8;rde-1* animals. *jyIs8* contains an integrated transgene that
191 expresses GFP under the control of the promoter of an OVIG, *pals-5*, and was used as a marker for
192 infection (Bakowski *et al.*, 2014). Uninfected controls established the absence of signal for *pals-*
193 *5p::GFP* and oRNA1 strands, while as in prior studies (Bakowski *et al.*, 2014), a strong signal in the
194 pharynx (asterisk) in the same channel as antigenome was observed from fluorescence of the *myo-*
195 *2p::mCherry* marker included in the *jyIs8* transgene (**Figure 2A; uninfected**). At 24hpi we saw robust
196 GFP expression in multiple intestinal cells that typically extended beyond the cell(s) that showed robust
197 signal with probes to genomic sequences. The multi-cell GFP expression is consistent with prior studies
198 showing distribution of DRH-1 and ZIP-1 beyond infected cells (Lažetić *et al.*, 2022; Batachari *et al.*,
199 2024). When we used antigenomic probes, ~95% of infected animals showed a diffuse cytoplasmic
200 signal without distinct puncta in the same intestinal cells that showed genomic signal (**Figures 2A,**
201 **infected (-) denature and 2B**). Given the requisite complementarity between OV strands, we
202 wondered if the observed signal was affected by basepairing. To test this, we treated animals with
203 50mM NaOH for ~30 seconds to promote dsRNA denaturation prior to hybridization (Genoyer *et al.*,
204 2025), hereafter referred to as denature-smFISH (dsmFISH). After denaturation, signal using genomic
205 probes was unchanged, consistent with the conventional understanding of replication of a positive
206 strand virus, whereby a vast excess of single-stranded genome is produced for subsequent packaging.
207 By contrast, after denaturation, in addition to the diffuse cytoplasmic signal, antigenomic probes
208 revealed a punctate signal in ~97% of infected animals (**Figures 2A, infected (+) denature and 2B**).
209 This indicated that the oRNA1 antigenomic signal derived from a species that was basepaired via
210 intramolecular or intermolecular interactions. We used the dsmFISH denaturing conditions for
211 subsequent experiments. Further, because the genomic signal was unaffected by denaturation, in
212 subsequent experiments we interpreted signal from genomic probes as corresponding to the single-
213 stranded genome quantified in our PCR experiments. The dependence of the antigenomic signal on
214 denaturation suggested the signal derived from a basepaired species, either the lowly abundant
215 antigenomic strand, viral dsRNA, or the viral siRNAs generated during antiviral RNAi.

216 Since the diffuse cytoplasmic signal observed with probes to the antigenome was similar to the
217 pattern of the oRNA1 genome signal, we wondered if the diffuse antigenomic signal was a
218 consequence of bleed-though from the genome channel. Thus, we monitored antigenome in infected
219 animals that had not been probed for genome, and vice-versa (**Figures 2C and 2D)**. We observed the
220 diffuse signal in the antigenome channel even when we only probed for genome, consistent with bleed-
221 through. In subsequent experiments we considered the diffuse cytoplasmic signal as nonspecific
222 background. However, a lower level of cytoplasmic signal, and importantly, distinct puncta, were
223 specific to antigenomic probes (**Figure 2C, white arrowhead**).

224 **Probes to the oRNA1 antigenome reveal perinuclear foci upon infection**

225 Having established optimal protocols, we performed more extensive analyses, now comparing
226 *jyIs8* (wildtype) with *jyIs8;rde-1* mutant animals at 24hpi. Again, infected intestinal cells showed robust
227 genomic signal as well as distinct puncta when using antigenomic probes (**Figure 3A**). *rde-1* mutant
228 animals exhibited more infected cells than wildtype as quantified by cytoplasmic genomic signal
229 (**Figure 3B**). Further, antigenomic probes revealed a distinct perinuclear signal, emphasized by line
230 scan analyses, in both wildtype and *rde-1* mutant strains (**Figure 3A)**; the perinuclear signal was only
231 observed after denaturation and was also observed when probes to the antigenome were used
232 exclusively, ruling out artifacts due to bleed-through (**Supplemental Figure 2**). Quantification showed
233 that in wildtype or *rde-1* mutant strains, ~83% or ~78% of infected animals exhibited perinuclear signal,
234 respectively (**Figure 3C**). The perinuclear puncta observed using antigenomic probes lacked an
235 obvious colocalizing genomic signal, but the line scan showed a peak of closely associated genomic
236 signal (**Figures 3D and 3E**). While the perinuclear puncta were the most common pattern observed
237 with the antigenomic probes, multiple biological replicates (≥10) revealed other patterns in infected
238 wildtype animals (**Figures 3F-J**). For example, close association of a punctate antigenomic signal with
239 genomic signal was observed in the cytoplasm (**Figures 3F and 3G**). In other cases, antigenomic
240 probes revealed concentrated cytoplasmic foci surrounded by genomic signal (**Figures 3H, white**
241 **arrowhead and 3I**). Given that antigenomic strand is used as a template for viral replication to
242 generate viral genome, possibly the closely associated genome and concentrated antigenomic puncta

243 indicates active replication hubs in the infected cytoplasm. In infected animals that only exhibited
244 genomic signal in the lumen **(Figure 3J**), as expected in animals that have released packaged virions
245 (Castiglioni *et al.*, 2024), we did not observe any cells with antigenomic signal, suggesting hybridizing
246 material was degraded or processed through antiviral defense mechanisms, or below limits of
247 detection.

248 **Primary siRNA biogenesis, but not secondary siRNA amplification, is required for perinuclear**
249 **signal**

250 A key aspect of antiviral defense in *C. elegans* is cleavage of viral dsRNA by the AVC, comprised of
251 DCR-1, DRH-1, and RDE-4 (Consalvo *et al.*, 2024). The AVC processes viral dsRNA to produce 23H
252 double-stranded 1° siRNAs (Reich *et al.*, 2018), and subsequently one strand of the 1° siRNA is bound
253 by RDE-1 for presentation to factors that amplify the siRNA response by producing single-stranded 22G
254 triphosphorylated 2° siRNAs. Mutations or deletions in DCR-1, DRH-1 or RDE-4 prevent accumulation
255 of both 1° and 2° siRNAs, while RDE-1 mutants accumulate 1° siRNAs but lack 2° siRNAs (Ashe *et al.*,
256 2013). In hopes of gaining insight into whether the perinuclear signal derived from full length
257 antigenome or siRNAs, we infected synchronized L1 larvae of *dcr-1(mg375), drh-1(uu60), rde-4(uu71),*
258 *rde-1(ne219)*, and wildtype (*N2*) animals for 24 hours and performed dsmFISH. As observed previously
259 (**Figure 2A, uninfected**), a minimal background of diffuse fluorescence in the antigenomic channel in
260 uninfected animals was observed for all strains (**Supplemental Figure 3**). At 24hpi, both wildtype and
261 RNAi mutants showed abundant genome signal in one or more intestinal cells, with significantly more
262 infected cells in RNAi mutants (**Figures 4A, G+AG column 1, and 4B**). Consistent with our previous
263 experiments, we observed distinct perinuclear signal with antigenomic probes in wildtype (~81%
264 animals) or *rde-1* mutants (~83% animals) (**Figures 4A and 4C, *N2, rde-1***). However, in animals
265 mutant for one of the three factors of the AVC, a fraction of animals showed a loss of perinuclear signal
266 (**Figures 4A and 4C, *dcr-1, drh-1, rde-4***). This result established a connection of the perinuclear signal
267 to processing by the AVC, albeit does not definitively determine whether the perinuclear signal derives
268 from the antigenome or antisense siRNAs. While animals with deficiencies in the AVC cannot process
269 viral dsRNA as efficiently as wildtype, some activity remains, for example, certain DRH-1 mutations

270 eliminate AVC processivity, but still generate siRNA reads that map to ends of the viral
271 genome/antigenome (Ashe *et al.*, 2013; Coffman *et al.*, 2017). Possibly residual siRNAs allow a
272 productive antiviral response in some but not all animals, explaining the reduction in animals with
273 perinuclear puncta. MUT-16 is a scaffolding component required for mutator foci formation in the
274 germline, sites where secondary siRNA amplification occurs (Phillips *et al.*, 2012; Uebel *et al.*, 2018).
275 MUT-16 is also required for 2° siRNA amplification during OV infection (Lowe *et al.*, 2025). We used a
276 *mut-16(pk710)* strain to test if this strain phenocopies *rde-1* mutants with respect to perinuclear
277 localization. We observed that over 85% of infected *mut-16* mutants at 24hpi exhibited perinuclear
278 signal, not significantly different from wildtype or *rde-1* mutant backgrounds (**Figures 4A and 4C, *mut-***
279 ***16***). Since *rde-1* and *mut-16* mutant animals, which accumulate 1° siRNAs but lack 2° siRNAs, show
280 robust perinuclear signal with antigenomic probes, our experiments suggest the perinuclear signal
281 requires wildtype accumulation of 1° siRNAs but is unaffected by aberrant accumulation of 2° siRNAs.
282 The 48 smFISH probes designed to bind antigenome, and the 27 that bind genome, were
283 distributed along the length of the antigenome and genome, respectively, and by overlaying viral siRNA
284 reads determined in a prior study (Ashe *et al.*, 2013), we noted probes that should hybridize with
285 positions of abundant viral siRNAs (**Supplemental Figures 4A-4D**); indeed, northern blot analyses
286 using these probes detected small viral siRNAs (22 or 23 nts) in 72hpi wildtype animals but not in RNAi
287 mutants (**Figure 4D**). We treated wildtype samples with “terminator”, which specifically degrades RNAs
288 with 5’ monophosphates such as 1°, but not 2°, siRNAs. Upon quantification, we did not observe any
289 significant difference in the levels of viral siRNA-sized products with terminator treatment (**Figure 4E**),
290 indicating that the siRNAs detected by northern blot were predominantly 2° siRNAs at 72hpi. While it is
291 difficult to compare the sensitivity of northern analyses with smFISH, these results suggest that 2°
292 siRNAs from oRNA1 would be easier to detect by imaging than 1° siRNAs, which is not surprising given
293 the abundance of 2° siRNAs (Ashe *et al.*, 2013; Dahal *et al.*, 2025). This combined with the lack of
294 changes in the perinuclear signal in RNAi mutants that should affect 2° siRNAs, supports the idea that
295 the perinuclear signal derives from antigenome or antisense 1° siRNAs.
296 **Perinuclear puncta do not colocalize with antiviral RNAi factors**

297 Given the loss of perinuclear antigenomic signal in a subset of animals with deficiencies in the AVC,
298 we considered the possibility that factors of the antiviral RNAi pathway (**Figure 5A**) might colocalize with
299 the perinuclear antigenomic signal. We took advantage of existing strains for DCR-1, RDE-1 and DRH-
300 3, a helicase related to DRH-1 that is involved in 2° siRNA amplification, that were tagged at the
301 endogenous locus with 3XFLAG::GFP. We observed a diffuse distribution of DCR-1, RDE-1 and DRH-3
302 without infection (**Figures 5B, 5C and 5D**). As expected from prior studies (Phillips *et al.*, 2012), in
303 uninfected and infected animals we observed DRH-3 localized at perinuclear foci in the germline which
304 served as an internal control (**Figure 5D**).
305 For all GFP-tagged proteins, DCR-1, RDE-1 and DRH-3, at 24hpi we observed distinct cytoplasmic
306 puncta in cells with genomic signal (**Figures 5E, 5G and 5H**), and these puncta were clearly separated
307 from perinuclear antigenomic puncta, as confirmed by line scan for DCR-1 (**Figures 5E and 5F**).
308 However, a few cytoplasmic DCR-1, RDE-1 or DRH-3 puncta colocalized with cytoplasmic antigenomic
309 puncta (**Figures 5E, 5G, and 5H**). Notably, DRH-1, a known interactor of DCR-1, also exhibits
310 cytoplasmic punctate distribution in OV-infected cells (Batachari *et al.*, 2024). The cytoplasmic punctate
311 pattern for DCR-1 was observed in 100% of infected animals, and for RDE-1 and DRH-3, in around 50%
312 of infected animals. Thus, although we observed that mutations in factors involved in the production of
313 1° siRNAs, but not those required for 2° siRNA amplification, showed reduced number of infected animals
314 with perinuclear antigenomic signal (**Figure 4C**), at least for the factors tested, we do not observe the
315 factors themselves localizing to the perinuclear region. Based on known mechanisms for antiviral RNAi,
316 where 1° siRNAs would be expected to be proximal to the factors that generate them, these results are
317 more consistent with the idea that perinuclear signal derives from the antigenome rather than 1° siRNAs;
318 importantly, it is also possible that we are observing a previously unrecognized step of antiviral RNAi.

319 **dsRNA accumulates during OV infection and associates with oRdRP**

320 Positive-strand viruses amplify their genome using the antigenome as template (Ball, 1994), and
321 viral dsRNA arises during this process. dsRNA is often visualized using dsRNA-specific antibodies (de
322 Faria *et al.*, 2023), and to understand if dsRNA accumulation varies in wildtype and RNAi mutants, we
323 used the J2 dsRNA-specific antibody with a dot blot assay, first showing that we could detect as low as

324 50pg of purified 800 basepair dsRNA (**Supplemental Figure 5**). We then collected total RNA from OV-
325 infected (72hpi) and uninfected samples and again used the dot blot assay to monitor dsRNA
326 accumulation. Control experiments showed that dsRNA was not detected without OV infection, and
327 consistent with the fact that wildtype animals have efficient antiviral RNAi, we also did not observe
328 dsRNA accumulation in wildtype animals (**Figure 6A**); however, given the limited sensitivity of this
329 assay, we cannot rule out the existence of low levels of dsRNA in the wildtype background. Importantly,
330 we detected dsRNA accumulation in all RNAi mutants tested (**Figure 6A**).

331 To evaluate whether the dsRNA signal was from viral or endogenous dsRNA, we looked for oRdRP
332 colocalized with dsRNA in infected cells. We infected *jyIs8* (wildtype) or *jyIs8;rde-1* animals, picked
333 GFP-positive infected animals and performed intestinal immunofluorescence assays using antibodies
334 against oRdRP and dsRNA (J2). We observed that *pals-5p::GFP* expressing infected intestinal cells
335 showed both oRdRP and dsRNA puncta, colocalized, in both *jyIs8* and *jyIs8;rde-1* animals (**Figure 6B;**
336 **red arrowhead**). We also observed a strong nuclear dsRNA signal in oRdRP containing *pals-5p::GFP*
337 expressing *jyIs8* intestinal cells that was not observed in uninfected animals or *jyIs8;rde-1* mutants
338 (**Figure 6B, merge zoom**). The dsRNA that is colocalized with oRdRP is consistent with viral dsRNA
339 being produced during replication, while the nuclear dsRNA more likely reflects endogenous intronic
340 dsRNA induced in infected animals (Reich *et al.*, 2018; Reich and Bass, 2019).

341 Interestingly, apart from oRdRP puncta, we noticed distinct oRdRP-containing spherical structures
342 in the *pals-5p::GFP* positive intestinal cells (**Figure 6B, merge zoom, white arrowhead**). Over 75% of
343 *pals-5p::GFP* positive wildtype animals exhibited at least one spherical oRdRP signal, with the rest only
344 showing oRdRP puncta (*p=0.0046*); less than 50% of *rde-1* mutant animals exhibited oRdRP spheres.
345 We quantified the total number of oRdRP spheres per animal and observed that wildtype animals
346 showed between 5 to 58 spheres with an average diameter of 1.023μm (**Figures 6C and 6D)**. The
347 number of spheres per animal was significantly lower in *jyIs8;rde-1* animals (*p=0.0424)*, with 0 to 25
348 spheres per animal and an average diameter of 1.122μm (*p=0.0154*), slightly higher than the observed
349 diameter in wildtype animals. While we did not observe any dsRNA puncta inside the oRdRP spherical
350 structures, we did find a few spheres closely associated with dsRNA puncta (**Figure 6B, merge zoom,**

351 **yellow arrowhead**). Overall, we report previously uncharacterized lumen-containing spherical
352 structures lined with oRdRP in wildtype background.

353 **Discussion**

354 The abnormal morphology of the intestine in RNAi mutant *C. elegans* after infection with OV has
355 been visualized with transmission electron microscopy (Félix *et al.*, 2011), and the OV genome and
356 oRdRP have been visualized using smFISH and immunofluorescence (Franz *et al.*, 2014; Castiglioni *et*
357 *al.*, 2024). Here we add to this understanding by characterizing OV replication intermediates that
358 include antigenomic sequences, dsRNA and oRdRP. Using quantitative, strand-specific methods, we
359 demonstrate genome is in vast excess of antigenome (**Figure 1**), as found in other positive-strand RNA
360 viruses (Novak and Kirkegaard, 1991; Félix *et al.*, 2011; Shulla and Randall, 2015; Warncke and
361 Knudsen, 2022; Genoyer *et al.*, 2025). By utilizing a helicase mutant of DCR-1 (*dcr-1(mg375)*), we
362 confirm the importance of helicase function to antiviral RNAi and efficient antiviral defense (**Figure 1;**
363 **Supplemental Figure 1**), as suggested previously by in vitro experiments (Consalvo *et al.*, 2024).
364 Probes designed to hybridize with viral antigenome allow unambiguous localization of the antigenome
365 after infection with most mammalian viruses (Shulla and Randall, 2015; Liu *et al.*, 2019; Genoyer *et al.*,
366 2025). However, in *C. elegans*, the existence of the antiviral RNAi pathway, which generates both
367 sense and antisense siRNAs, precludes a straightforward interpretation of signal from hybridization to
368 antigenomic probes. Here we take the first steps to address this issue, showing that denaturation
369 protocols are required for detection of antigenomic, but not genomic, sequences in infected cells, and
370 that antigenomic probes reveal both cytoplasmic and perinuclear signal, with the later altered in animals
371 defective for 1°, but not 2°, siRNA pathways. We also report that oRdRP is present at the surface of
372 lumen-containing spheres, and a decrease in the number of spheres in *rde-1* mutants suggests
373 spheres may be related to host clearance of viral byproducts (**Figures 6B, 6C**). Our study offers an
374 example of an invertebrate viral infection model and sets the stage for a more complete spatial and
375 temporal understanding of the OV life cycle and host responses.

376 **What replication intermediates are detected with OV antigenomic probes?**

377 Our studies establish the conditions necessary for detecting OV antigenomic sequences, but as
378 yet, we cannot definitively assign the signal acquired with antigenomic probes as arising from
379 antigenome or the antisense strand of an siRNA. That said, by comparison to known paradigms, in
380 some cases we can choose the most parsimonious conclusion. For example, during infection with
381 +ssRNA viruses, the antigenome is typically restricted to regions of viral replication in the cytoplasm
382 (den Boon *et al.*, 2024), and our observation of cytoplasmic antigenomic signal after OV infection is
383 consistent with this. However, in addition to cytoplasmic puncta, using dsmFISH, we observed ~80% of
384 OV-infected wildtype animals with a perinuclear signal using antigenomic probes (**Figure 7A**), without
385 the presence of other signatures of replication, such as oRdRP, genome, or dsRNA (**Figures 3A and**
386 **6B**). In the *C. elegans* germline, perinuclear regions are hubs for RNAi machinery (Phillips *et al.*, 2012;
387 Huang *et al.*, 2024), but so far, such perinuclear granules have not been observed in somatic tissues,
388 and we did not observe association of perinuclear antigenome with a subset of known RNAi factors
389 (DCR-1, RDE-1, DRH-3; **Figures 5E, 5G, 5H**). Of course, there are other factors involved in steps in
390 between RDE-1 loading and 2° siRNA amplification, such as RDE-8 (Tsai *et al.*, 2015), and also in the
391 subsequent targeting of the genome for degradation, which requires SAGO-2 (Seroussi *et al.*, 2023),
392 and it remains possible that these factors or others will be associated with the perinuclear antigenome.
393 One of our most important observations in regard to the perinuclear antigenomic signal is that
394 these puncta were dependent on the AVC factors required for producing 1° siRNAs (DCR-1, DRH-1,
395 RDE-4) (**Figure 7B**) but are not affected by factors required for secondary siRNA biogenesis (RDE-1,
396 MUT-16; **Figures 4A, 4C, 7C**). Regardless of whether the perinuclear signal results from 1° siRNAs or
397 the OV antigenome, this indicates an important connection between OV infection and antiviral RNAi.
398 As evident from our strand-specific RT-qPCR assays, we observed a moderate increase in the
399 antigenomic strand abundance in RNAi mutants relative to WT (**Figures 1D and 1E**). Thus, it is also
400 possible that the loss of antigenomic perinuclear signal in primary RNAi mutants might correlate with an
401 increased antigenomic signal in the cytoplasm, suggesting an impaired localization (**Figure 4A**). While
402 images appear to suggest this, further quantification is necessary to conclude whether the increased
403 cytoplasmic signal compensates for the signal from the perinuclear region in these mutants.

404 **What is the nature of dsRNA induced during OV infection?**

405 During infection by both DNA and RNA viruses, dsRNA accumulates in infected cells, typically in
406 the cytoplasm (Son *et al.*, 2015). The large majority of existing studies detect dsRNA using
407 commercially available antibodies (Corbet *et al.*, 2022; de Faria *et al.*, 2023), and the dsRNA is inferred
408 to be of viral origin because it correlates with infection, and in some cases is observed associated with
409 the viral RdRP (Andronov *et al.*, 2024). Indeed, using an antibody to dsRNA, we and others have
410 observed dsRNA accumulation in OV-infected intestinal cells (**Figure 6B;** (Batachari *et al.*, 2024)).
411 Previous observations of oRdRP show a cytoplasmic distribution in OV-infected cells (Franz *et al.*,
412 2014), and in our studies, in wildtype and *rde-1* mutant animals, we find cytoplasmic dsRNA puncta
413 associated with oRdRP, consistent with a viral origin (**Figure 6B**). These dsRNA-associated oRdRP
414 puncta are possible viral replication hubs, similar to previous observations in other +ssRNA virus
415 infections (Shulla and Randall, 2015; Andronov *et al.*, 2024). We also observed closely associating
416 genome and antigenome cytoplasmic puncta suggestive of replication hubs (**Figures 3F and 3H**). In
417 future studies it will be important to determine whether antigenome can be observed to colocalize with
418 oRdRP to confirm the presence of cytoplasmic replication hubs. dsRNA puncta that lack association
419 with oRdRP could be partially processed dsRNAs or siRNAs as J2 can also recognize dsRNA as short
420 as 14bp albeit with less affinity (Bou-Nader *et al.*, 2025).

421 As in prior studies that used antibodies to detect dsRNA after viral infection of mammalian cells
422 (Son *et al.*, 2015), we also observed dsRNA in the nucleus. A robust nuclear J2 signal was observed
423 only after viral infection (**Figure 6B, *jyIs8*, dsRNA**), in *pals-5p::GFP* positive cells, but not in
424 neighboring *pals-5p::GFP* negative cells. While it is possible that this dsRNA is of viral origin, we favor
425 the idea that it derives from infection-induced transcription of endogenous genes that contain intronic
426 dsRNA, which are prevalent in many animals (Reich and Bass, 2019). Among the differentially-
427 expressed genes produced during OV infection (Chen *et al.*, 2017; Castiglioni *et al.*, 2024), some do
428 contain introns that encode dsRNA, such as *zip-1* and *uggt-2*, as defined in Reich et.al. (Reich *et al.*,
429 2018). Interestingly the nuclear dsRNA signal is observed in wildtype-infected nuclei but not in *rde-1*
430 animals (**Figure 6B**), possibly due to their inefficient antiviral response. This also highlights the

431 importance of investigating antiviral responses in a wildtype background, since unique host responses
432 to OV may not always be evident in mutant strains.

433 **What are oRdRP spheres?**

434 Prior studies have only visualized oRdRP in RNAi mutant backgrounds at late larval stages,
435 possibly explaining why these spherical structures were missed previously (Franz *et al.*, 2014). While
436 typical viral replication organelles are ~300nm in diameter, we observed oRdRP-rimmed spheres
437 (**Figures 6B**), that were larger, ~1μm in diameter (**Figure 6D**), and in contrast to replication organelles,
438 lacked association with dsRNA (**Figure 6B**). Further, even though *rde-1* mutant animals are more
439 permissive to virus, they exhibited reduced oRdRP spheres (**Figures 6B and 6C**), consistent with the
440 idea that spheres are not replication organelles. While higher resolution analyses are required to
441 determine the nature and function of oRdRP sphere interaction with cellular organelles, one intriguing
442 possibility is that these are structures associated with clearance, since viral RdRPs of +ssRNA viruses
443 are not typically packaged into virions. Possibly, the oRdRP spheres we observe at 24hpi (**Figure 6B**)
444 are formed from the remnants of replication sites targeted by the host for clearance after efficient
445 antiviral defense (**Figure 7D**), which would be impaired in *rde-1* mutants (**Figure 7E**). In other viral
446 infection models, viral RdRP is ubiquitinated and degraded through autophagy or proteosome
447 degradation pathways (Liang *et al.*, 2021), and between 12hpi and 24hpi with OV, genes related to
448 ubiquitin-proteasome pathways are induced (Chen *et al.*, 2017; Castiglioni *et al.*, 2024). In *C. elegans*,
449 infection with OV also induces GFP::LGG-1 puncta, which shows partial association with ubiquitin
450 puncta (Bakowski *et al.*, 2014). It will be important in future studies to determine whether or not the
451 oRdRP in spheres is ubiquitinated by the host machinery and targeted for degradation through
452 autophagy post viral replication.

453 **Materials and Methods**

454 ***C. elegans* growth and maintenance**

455 All *C. elegans* strains were cultured at 20°C under standard conditions unless specified (Brenner,
456 1974). The list of strains used in this study can be found in S1 Table. Some strains were provided by
457 the CGC, which is funded by NIH Office of Research Infrastructure Programs (P40 OD010440).

458 **Orsay virus filtrate preparation**

459 OV filtrate was prepared, and viral titer calculated, as described (Jiang *et al.*, 2017). Briefly, JU1580
460 strain was cultured in S medium (T, 2006) and infected with OV for 3 days. Following infection,
461 supernatant was collected and passed through a 0.22μm filter. The resulting filtrate was aliquoted and
462 flash frozen at -80°C for long term storage. To calculate viral titer, *rde-1(ne219)* animals (1000 L1 per
463 plate) were infected with serial dilutions (10-fold dilutions prepared in M9 buffer) of the viral filtrate.

464 **Orsay virus infection**

465 For viral load, strand-specific PCR (ss-qPCR), northern blot and dot blot experiments: Strains were
466 grown to gravid adults in liquid medium. Gravid adults were bleached (10% NaOH, 20% bleach), and
467 embryos were synchronized in M9 buffer overnight at 20°C. For L3 infection experiments, 2000
468 synchronized L1s were plated in OP50-containing NGM plates and grown for 39 hours at 20° and
469 infected with 0.1X OV for either 12 hours or 24 hours. For L1 infection experiments, 2000 synchronized
470 L1s were plated in OP50-containing NGM plates and infected with 0.1X OV for 48 or 72 hours. The
471 resulting infected and uninfected animals were washed in M9 buffer 4 times and collected in Trizol for
472 RNA extraction.

473 For intestinal dissection: ~200 synchronized L1 animals were transferred to a plate containing OP50.
474 Animals were incubated for 44-48 hours until they reached late larval stage (L3/L4). Animals were
475 infected with OV (0.1X or 1X) for 24 hours and collected for dissections.

476 For smFISH experiments: ~300-500 synchronized L1s of respective strains were plated on OP50-
477 containing plates and infected with OV (1X) at 20°C. Infected animals were collected after 24 hours of
478 infection.

479 **RNA extraction, cDNA synthesis and qPCR**

480 Total RNA from worms was collected using Trizol-chloroform-isopropanol extraction. Briefly, animals
481 frozen in Trizol were thawed, and chloroform was added. Aqueous layer was separated, and RNA was
482 precipitated using 100% isopropyl alcohol by incubating at room temperature for 30 minutes. The
483 resulting pellet was washed and treated with DNase. DNase-treated RNA was then purified using Zymo
484 RNA pure column as per manufacturer's instructions. The resulting total RNA was used for all
485 downstream analyses. cDNA was synthesized using Applied Biosystems cDNA synthesis kit as per
486 manufacturer's protocol for all experiments involving random hexamers. qPCR was performed using a
487 QuantStudio3 instrument. Primers for qPCR are listed in S2 Table. Ct values were normalized to levels
488 of *cdc-42*, and fold change was calculated using the ΔΔCt method (Livak and Schmittgen, 2001).

489 **Strand-specific RT-qPCR**

490 We used strand-specific probes designed to bind the middle of one of the two Orsay RNA1 (oRNA1)
491 strands; each probe also included a unique adapter sequence that did not bind within the viral genome
492 or antigenome. To synthesize first strand cDNA, we incubated the probe with RNA and 10mM dNTP at
493 60°C for 10 mins, followed by reverse transcription at 37°C for 1 hour using the Applied Biosystems
494 cDNA synthesis kit; enzyme was inactivated at 85°C for 20 minutes. We then used this strand-specific
495 cDNA for qPCR. The unique adapter sequence was used as a forward primer combined with a reverse
496 primer complementary to a region on the same strand of oRNA1, for qPCR. Primers are listed in S3
497 Table.

498 **Dot blot assay**

499 Dot blot assays were performed as described (de Faria *et al.*, 2023) with slight modifications. Briefly,
500 500ng of total RNA was diluted to 4μl and carefully spotted onto a supercharged nylon membrane.
501 Once dried, the membrane was crosslinked under UV light (UV Stratalinker 1800, auto-crosslink
502 setting). The cross-linked membrane was blocked in blocking buffer (1X PBS, 0.05% Tween-20,
503 50mg/ml sheared salmon sperm DNA, 5% skim milk) for 1 hour at room temperature (RT). The
504 membrane was incubated with primary antibody (Anti-dsRNA:J2, 1:2000) overnight at 4°C. The
505 membrane was then washed thrice with 1X PBST (1X PBS, 0.05% Tween-20) for 10 minutes at RT.
506 The membrane was then incubated with secondary antibody (Anti-mouse IR dye 800CW, 1:20,000) for

507 1 hour at RT. The membrane was washed twice with 1XPBST for 10 minutes at RT, followed by two
508 washes with 1X PBS for 10 minutes at RT. The membrane was then imaged using a LI-COR Odessey
509 Infrared Imager. Antibodies were diluted in antibody dilution buffer (1X PBS, 0.05% tween-20, 2% skim
510 milk). In-vitro synthesized and gel-purified ~800bp dsRNA was used as control for the dot blot assay.

511 **Intestine dissection, immunostaining**

512 Dissection and immunostaining protocols were based on (Batachari *et al.*, 2024) with modifications as
513 below. Briefly, GFP+ infected animals were picked onto 20μl of 5μM levamisole. Worms were dissected
514 using sterilized surgical blades and transferred to 1X M9 buffer. Dissected intestines were washed
515 twice with 1X M9, twice with 1X PBST and fixed in 4% paraformaldehyde at RT for 15 minutes. Fixed
516 intestines were washed thrice with 1X PBST and blocked using a blocking solution (1X PBS, 0.5%
517 Tween-20, 5% Bovine Serum Albumin, 0.5% Sodium azide) at 4°C overnight. Following blocking,
518 intestines were incubated with Anti-oRdRP antibody (gift from Dr. David Wang (Franz *et al.*, 2014)) and
519 Anti-dsRNA (J2) antibody for 1-2 hours at RT. Unbound primary antibodies were washed off with 1X
520 PBST, followed by incubation with secondary antibodies for 1-2 hours at RT. This was followed by two
521 washes with 1X PBST and one wash with 1X PBST containing Hoechst (0.1ng/mL). For lipid droplet
522 staining, LipidSpot™ 610 Lipid droplet stain was diluted in 1X PBST and incubated for 30mins before
523 Hoechst staining. Immunostained intestines were stored in 1X PBST at 4°C until mounting and imaging.
524 Antibodies were diluted in blocking solution as per manufacturer's recommendations. Antibody
525 information is listed in S3 Table.

526 **smFISH**

527 ~200 synchronized L1s of *jyIs8* or *jyIs8;rde-1* were plated on OP50-containing plates and infected with
528 OV at 20°C. Infected animals were collected after 24 hours of infection. Animals were washed with 1X
529 M9 buffer and 1X PBST (1X PBS, 0.05% Tween-20) and then fixed in 4% paraformaldehyde for 15
530 minutes at RT. Fixed animals were washed thrice with 1X PBST, followed by permeabilization in 70%
531 ethanol in 1X PBST for at least 2 hours at 4°C. Permeabilized worms were washed thrice with 1X PBST
532 to remove residual ethanol. If applicable, denaturation of dsRNA was performed by treating worms with
533 50mM sodium hydroxide for ~30 seconds at RT (Genoyer *et al.*, 2025) and immediately washing twice

534 with 1X PBST. This was followed by a wash with 2X SSC buffer (Saline-Sodium Citrate), and then
535 animals were pre-hybridized in 1 mL of Wash Buffer A (Stellaris® RNA FISH Wash Buffer A with
536 nuclease-free water and 10% formamide). Samples were then hybridized to probes for the genome (27
537 probes) and antigenome (48 probes) (1μl of 12.5μM of each probe mix) in 100μl of hybridization buffer
538 (Stellaris® RNA FISH Hybridization buffer with freshly added 10% formamide) per sample. Samples
539 were incubated at 37°C overnight at 1200rpm (vortex). Post-hybridization, Wash Buffer A was directly
540 added to samples followed by incubation at 37°C for 30 minutes (vortex). Pellet was washed with Wash
541 Buffer A with Hoechst (0.1ng/mL) at 37'C or 30 minutes (vortex), followed by Stellaris® RNA FISH
542 Wash Buffer B for 5 mins at RT on the nutator and then washed once with 1X PBST. Hybridized
543 samples were stored in 1X PBST at 4°C until imaging. The sequences of the smFISH probes are listed
544 in S4 Table.

545 **Imaging**

546 Animals were mounted onto 2% agarose pads using Vectashield mounting solution. Images were
547 captured using a DeltaVision Widefield Microscope with a 60X (oil) objective, Numerical Aperture
548 (NA=1.42), equipped with a sCMOS digital camera using the Blue-Green-Orange-Far Red channels or
549 Blue-Green-Red-Far Red channels. Multiple Z-slices spanning the entire thickness of the intestine with
550 Z-stacks 0.2μM apart were captured. Images were captured and deconvolved using the softWoRx
551 image processing software using standard settings. Individual channels were minimally adjusted in FIJI
552 for better visualization. Unless otherwise specified, a single Z-slice was used to represent data.
553 Acquisition setting for smFISH: Genome (Far-red), 5% transmission, 0.015-0.075 second exposure.
554 Antigenome (Orange), 30-50%transmission, 0.200-0.500 second exposure. Note that antigenome
555 channel was exposed for at least 10X longer than the genome channel.

556 **Quantification of perinuclear puncta distribution of oRNA1 antigenome**

557 Deconvolved and processed images were opened on ImageJ, and colors were assigned for genome
558 (cyan) and antigenome (magenta) channels. A composite image was created with a merge of these
559 channels. Animals with at least one perinuclear puncta enriched for antigenome and negative for

560 genome were considered a positive hit (visualized through line scan analysis). Randomization and blind
561 quantification were performed with the help of Bass lab members to account for user bias.

562 **Quantification of oRdRP spheres**

563 Deconvolved and processed images were used to perform oRdRP sphere diameter quantification on
564 minimally adjusted Z-slices for the oRdRP channel. Progressive z-slices showing a point progressing to
565 a circle and ending back in a point, was considered a sphere. Center z-slice of the sphere was
566 determined, and the diameter (from a single z-slice) was calculated using the line tool on ImageJ.
567 Randomization and blind quantification were performed with the help of Bass lab members to account
568 for user bias.

569 **Heat shock inducible transgenic replicon system: heat shock induction protocol**

570 Transgenic array, GFP positive (in pharynx) animals (4-5 L4s) were picked onto a fresh OP50-
571 containing plate. Animals were incubated at 20°C for 3 days. Once they reached L4 larval stage,
572 animals were heat shocked at 34°C for 2 hours. Animals were collected after 24 hours of recovery at
573 20°C for strand-specific RT-qPCR and northern blot assays.

574 **Standard curve for strand-specific RT-qPCR**

575 In the region where the strand-specific primers were designed to bind oRNA1, a 500bp region was
576 amplified using primers flanking a T7 promoter (genome) or SP6 promoter (antigenome). The purified
577 PCR product was then used for in-vitro transcription to generate the genomic or antigenomic strand
578 using T7 or SP6 RNA polymerase, respectively. Known numbers of purified ssRNA strands, ranging
579 from 10^9 to 10^2 copies, were used for reverse transcription using strand-specific primers to generate
580 cDNA. The resulting cDNA was used for qPCR to generate a standard curve with copy number on the
581 x-axis and cycle threshold (Ct) values on the y-axis. Standard curve was generated, and the equation
582 was obtained by fitting points to a semi-log line using GraphPad Prism software. The resulting equation
583 was then used to determine copy number for strand-specific RT-qPCR analysis of infection
584 experiments.

585 **Northern blot**

586 Total RNA purified from early and late infected animals was heated at 65°C for 10 minutes in northern
587 loading buffer containing ethidium bromide. Long transcripts (genome and antigenome) were resolved
588 in agarose gel, while small RNAs were resolved in polyacrylamide-urea (17%(19:1), 8M Urea) gel.
589 Buffers were prepared and northern blot was performed as described in (He, 2013). Membrane was
590 then imaged under short UV light to capture ethidium bromide staining for the loading control.
591 Membrane was pre-hybridized using hybridization buffer at 42°C for 20-30 minutes. 50μL purified, and
592 end-labeled probes were mixed with hybridization buffer and added to the membrane for hybridization
593 overnight at 42°C (37°C for siRNA probing); membranes were then washed with northern wash buffer
594 thrice. Antigenome hybridized membranes were exposed to a PhosphorImager screen for 3 days;
595 genome hybridized membranes were exposed for 2-3 hours; 72hpi sample containing membrane was
596 only exposed for 15 minutes, viral siRNA probe-hybridized membranes were exposed overnight, U6
597 snRNA was visualized after 15minutes of exposure. PhosphorImage screens were imaged with a
598 Typhoon Biomolecular Imager. The sequences of the northern blot probes are listed in S5 Table.
599 **CRISPR-Cas9 for *rde-4(uu71)* generation**
600 *rde-4(uu71)* allele was generated with the CRISPR/Cas9 system as described (Reich *et al.*, 2018).
601

602 **Acknowledgements**

603 We thank Bass lab members for helpful discussions and feedback. We thank Ryan Andrews for initial
604 help with imaging of smFISH experiments. We thank Adam Hughes, Minna Roh-Johnson, Nidhi
605 Raghuram, Ofer Rog and Sara Wong for helpful suggestions and feedback on microscopy data and
606 methods. We acknowledge the Cell Imaging Core at the University of Utah for use of equipment
607 (DeltaVision Ultra Widefield Microscope). Anti-RdRP (OV) antibody was a kind gift from Dr. David
608 Wang. This work wias supported by funding to B.L.B. from the National Institute of General Medical
609 Sciences (R35GNaM141262) and the National Cancer Institute of the National Institutes of Health
610 (R01CA260414). B.L.B. is a Jon M. Huntsman Presidential Endowed Chair.

611 **References**

612 Ahlquist, P, Noueiry, AO, Lee, W-M, Kushner, DB, and Dye, BT (2003). Host Factors in Positive-Strand
613 RNA Virus Genome Replication. J Virol 77, 8181–8186.

614 Andronov, L, Han, M, Zhu, Y, Balaji, A, Roy, AR, Barentine, AES, Patel, P, Garhyan, J, Qi, LS, and
615 Moerner, WE (2024). Nanoscale cellular organization of viral RNA and proteins in SARS-CoV-2
616 replication organelles. Nat Commun 15, 4644.

617 Ashe, A, Bélicard, T, Le Pen, J, Sarkies, P, Frézal, L, Lehrbach, NJ, Félix, M-A, and Miska, EA (2013). A
618 deletion polymorphism in the Caenorhabditis elegans RIG-I homolog disables viral RNA dicing and
619 antiviral immunity. eLife 2, e00994.

620 Bakowski, MA, Desjardins, CA, Smelkinson, MG, Dunbar, TA, Lopez-Moyado, IF, Rifkin, SA, Cuomo,
621 CA, and Troemel, ER (2014). Ubiquitin-Mediated Response to Microsporidia and Virus Infection in C.
622 elegans. PLOS Pathog 10, e1004200.

623 Ball, LA (1994). Replication of the genomic RNA of a positive-strand RNA animal virus from negative-
624 sense transcripts. Proc Natl Acad Sci U S A 91, 12443–12447.

625 Batachari, LE, Dai, AY, and Troemel, ER (2024). Caenorhabditis elegans RIG-I-like receptor DRH-1
626 signals via CARDs to activate antiviral immunity in intestinal cells. Proc Natl Acad Sci 121,
627 e2402126121.

628 de Beijer, NL, Snijder, EJ, and Bárcena, M (2024). A Cool Look at Positive-Strand RNA Virus
629 Replication Organelles: New Insights from Cryo-Electron Microscopy. Annu Rev Biochem 93, 163–187.

630 den Boon, JA, Nishikiori, M, Zhan, H, and Ahlquist, P (2024). Positive-strand RNA virus genome
631 replication organelles: structure, assembly, control. Trends Genet TIG 40, 681–693.

632 Bou-Nader, C, Juma, KM, Bothra, A, Brasington, AJ, Ghirlando, R, Suzuki, M, Garboczi, DN, Leppla,
633 SH, and Zhang, J (2025). Specificity and mechanism of the double-stranded RNA-specific J2
634 monoclonal antibody. 2025.05.09.649859.

635 Brenner, S (1974). The Genetics of CAENORHABDITIS ELEGANS. Genetics 77, 71–94.

636 Castiglioni, VG, Olmo-Uceda, MJ, Villena-Giménez, A, Muñoz-Sánchez, JC, Legarda, EG, and Elena,
637 SF (2024). Story of an infection: Viral dynamics and host responses in the Caenorhabditis elegans-
638 Orsay virus pathosystem. Sci Adv 10, eadn5945.

639 Chen, K, Franz, CJ, Jiang, H, Jiang, Y, and Wang, D (2017). An evolutionarily conserved transcriptional
640 response to viral infection in Caenorhabditis nematodes. BMC Genomics 18.

641 Coffman, SR, Lu, J, Guo, X, Zhong, J, Jiang, H, Broitman-Maduro, G, Li, W-X, Lu, R, Maduro, M, and
642 Ding, S (2017). Caenorhabditis elegans RIG-I Homolog Mediates Antiviral RNA Interference
643 Downstream of Dicer-Dependent Biogenesis of Viral Small Interfering RNAs. mBio 8.

644 Consalvo, CD, Aderounmu, AM, Donelick, HM, Aruscavage, PJ, Eckert, DM, Shen, PS, and Bass, BL
645 (2024). C. elegans Dicer acts with the RIG-I-like helicase DRH-1 and RDE-4 to cleave dsRNA. eLife 13.

646 Corbet, GA, Burke, JM, Bublitz, GR, Tay, JW, and Parker, R (2022). dsRNA-induced condensation of
647 antiviral proteins modulates PKR activity. Proc Natl Acad Sci 119, e2204235119.

648 Dahal, K, Xia, M, Lu, J, Yan, T, and Lu, R (2025). Characterizing the role of RSD-6 in the biogenesis of
649 virus-derived small interfering RNAs and the modulation of viral pathogenesis. J Virol.

650 de Faria, IJS, Imler, J-L, and Marques, JT (2023). Protocol for the analysis of double-stranded RNAs in
651 virus-infected insect cells using anti-dsRNA antibodies. STAR Protoc 4, 102033.

652 Félix, M-A, Ashe, A, Piffaretti, J, Wu, G, Nuez, I, Bélicard, T, Jiang, Y, Zhao, G, Franz, CJ, Goldstein,
653 LD, *et al.* (2011). Natural and Experimental Infection of Caenorhabditis Nematodes by Novel Viruses
654 Related to Nodaviruses. PLOS Biol 9, e1000586.

655 Félix, M-A, and Wang, D (2019). Natural Viruses of Caenorhabditis Nematodes. Annu Rev Genet 53,
656 313–326.

657 Franz, CJ, Renshaw, H, Frezal, L, Jiang, Y, Félix, M-A, and Wang, D (2014). Orsay, Santeuil and Le
658 Blanc viruses primarily infect intestinal cells in *Caenorhabditis* nematodes. Virology 448, 255–264.

659 Genoyer, E, Wilson, J, Ames, JM, Stokes, C, Moreno, D, Etzyon, N, Oberst, A, and Gale, M (2025).
660 Exposure of negative-sense viral RNA in the cytoplasm initiates innate immunity to West Nile virus. Mol
661 Cell 85, 1147-1161.e9.

662 Guo, X, Zhang, R, Wang, J, Ding, S-W, and Lu, R (2013). Homologous RIG-I–like helicase proteins
663 direct RNAi-mediated antiviral immunity in C. elegans by distinct mechanisms. Proc Natl Acad Sci U S
664 A 110, 16085–16090.

665 He, SL (2013). Northern blot. Methods Enzymol 530, 75–87.

666 Huang, X, Feng, X, Yan, Y, Xu, D, Wang, K, Zhu, C, Dong, M, Huang, X, Guang, S, and Chen, X
667 (2024). Compartmentalized localization of perinuclear proteins within germ granules in C. elegans.
668 2024.03.25.586584.

669 Jakubiec, A, and Jupin, I (2007). Regulation of positive-strand RNA virus replication: The emerging role
670 of phosphorylation. Virus Res 129, 73–79.

671 Jiang, H, Chen, K, Sandoval, LE, Leung, C, and Wang, D (2017). An Evolutionarily Conserved Pathway
672 Essential for Orsay Virus Infection of Caenorhabditis elegans. mBio 8.

673 Lažetić, V, Wu, F, Cohen, LB, Reddy, KC, Chang, Y-T, Gang, SS, Bhabha, G, and Troemel, ER (2022).
674 The transcription factor ZIP-1 promotes resistance to intracellular infection in Caenorhabditis elegans.
675 Nat Commun 13, 17.

676 Liang, S, Wu, Y-S, Li, D-Y, Tang, J-X, and Liu, H-F (2021). Autophagy in Viral Infection and
677 Pathogenesis. Front Cell Dev Biol 9.

678 Liu, D, Tedbury, PR, Lan, S, Huber, AD, Puray-Chavez, MN, Ji, J, Michailidis, E, Saeed, M, Ndongwe,
679 TP, Bassit, LC, *et al.* (2019). Visualization of Positive and Negative Sense Viral RNA for Probing the
680 Mechanism of Direct-Acting Antivirals against Hepatitis C Virus. Viruses 11, 1039.

681 Livak, KJ, and Schmittgen, TD (2001). Analysis of relative gene expression data using real-time
682 quantitative PCR and the 2(-Delta Delta C(T)) Method. Methods San Diego Calif 25, 402–408.

683 Lowe, D, Shukla, A, and Kennedy, S (2025). Viral RNA pUGylation Promotes Antiviral Immunity in C.
684 elegans. 2025.07.09.663919.

685 Novak, JE, and Kirkegaard, K (1991). Improved method for detecting poliovirus negative strands used
686 to demonstrate specificity of positive-strand encapsidation and the ratio of positive to negative strands
687 in infected cells. J Virol 65, 3384–3387.

688 Pavelec, DM, Lachowiec, J, Duchaine, TF, Smith, HE, and Kennedy, S (2009a). Requirement for the
689 ERI/DICER complex in endogenous RNA interference and sperm development in Caenorhabditis
690 elegans. Genetics 183, 1283–1295.

691 Pavelec, DM, Lachowiec, J, Duchaine, TF, Smith, HE, and Kennedy, S (2009b). Requirement for the
692 ERI/DICER Complex in Endogenous RNA Interference and Sperm Development in Caenorhabditis
693 elegans. Genetics 183, 1283–1295.

694 Phillips, CM, Montgomery, TA, Breen, PC, and Ruvkun, G (2012). MUT-16 promotes formation of
695 perinuclear Mutator foci required for RNA silencing in the C. elegans germline. Genes Dev 26, 1433–
696 1444.

697 Reddy, KC, Dror, T, Sowa, JN, Panek, J, Chen, K, Lim, ES, Wang, D, and Troemel, ER (2017). An
698 Intracellular Pathogen Response Pathway Promotes Proteostasis in C. elegans. Curr Biol CB 27, 3544-
699 3553.e5.

700 Reich, DP, and Bass, BL (2019). Mapping the dsRNA World. Cold Spring Harb Perspect Biol 11,
701 a035352.

702 Reich, DP, Tyc, KM, and Bass, BL (2018). C. elegans ADARs antagonize silencing of cellular dsRNAs
703 by the antiviral RNAi pathway. Genes Dev 32, 271–282.

704 Seroussi, U, Lugowski, A, Wadi, L, Lao, RX, Willis, AR, Zhao, W, Sundby, AE, Charlesworth, AG,
705 Reinke, AW, and Claycomb, JM (2023). A comprehensive survey of C. elegans argonaute proteins
706 reveals organism-wide gene regulatory networks and functions. eLife 12, e83853.

707 Shulla, A, and Randall, G (2015). Spatiotemporal analysis of hepatitis C virus infection. PLoS Pathog
708 11, e1004758.

709 Son, K-N, Liang, Z, and Lipton, HL (2015). Double-Stranded RNA Is Detected by Immunofluorescence
710 Analysis in RNA and DNA Virus Infections, Including Those by Negative-Stranded RNA Viruses. J Virol
711 89, 9383–9392.

712 Sowa, JN, Jiang, H, Somasundaram, L, Tecle, E, Xu, G, Wang, D, and Troemel, ER (2019). The C.
713 elegans RIG-I homolog DRH-1 mediates the Intracellular Pathogen Response upon viral infection. J
714 Virol.

715 Stancheva, VG, and Sanyal, S (2024). Positive-strand RNA virus replication organelles at a glance. J
716 Cell Sci 137, jcs262164.

717 T, S (2006). Maintenance of C. elegans. WormBook Online Rev C Elegans Biol.

718 Tsai, H-Y, Chen, C-CG, Conte, D, Moresco, JJ, Chaves, DA, Mitani, S, Yates, JR, Tsai, M-D, and Mello,
719 CC (2015). A ribonuclease coordinates siRNA amplification and mRNA cleavage during RNAi. Cell 160,
720 407–419.

721 Uebel, CJ, Anderson, DC, Mandarino, LM, Manage, KI, Aynaszyan, S, and Phillips, CM (2018). Distinct
722 regions of the intrinsically disordered protein MUT-16 mediate assembly of a small RNA amplification
723 complex and promote phase separation of Mutator foci. PLOS Genet 14, e1007542.

724 Warncke, SR, and Knudsen, CR (2022). Detection methods targeting the positive- and negative-sense
725 RNA transcripts from plus-stranded RNA viruses. APMIS Acta Pathol Microbiol Immunol Scand 130,
726 284–292.

727 Welker, NC, Pavelec, DM, Nix, DA, Duchaine, TF, Kennedy, S, and Bass, BL (2010). Dicer's helicase
728 domain is required for accumulation of some, but not all, C. elegans endogenous siRNAs. RNA 16,
729 893–903.

730

731 **Figure 1: Dynamics of oRNA1 strand-specific accumulation upon OV infection.**

732 (A) Schematic of strand-specific RT-qPCR of OV RNA1. Primers with unique adapters (green colors)
733 were used for reverse transcription to generate cDNA specifically from oRNA1 strands. Resulting cDNA
734 was used for qPCR with primers that recognize the unique adapter and a downstream region (in black,
735 half arrows). Schematics of (B) late larval (L3) and (C) early larval (L1) OV infection protocols. Number
736 of copies (per ng of total RNA) of oRNA1 genome and antigenome at (D) L3 or (E) L1 infection of
737 indicated strains and times. Data, mean with standard deviation (N=3, biological replicates). Black
738 asterisks, significance between indicated infection time point and previous time point for oRNA1
739 genomic strand; Two-way ANOVA, Uncorrected Fischer's LSD test. Pink asterisks, significance
740 between genome and antigenome at indicated timepoint as shown for N2; Ratio paired t-test. No
741 asterisks, no significant difference (See also S1 Fig). Number of copies of oRNA1 genome or
742 antigenome as measured by strand-specific RT-qPCR in (F) constitutively OV-infected JU1580 animals
743 (Dotted lines, copy number of genome or antigenome in N2 animals at 12hpi. Ratio paired t-test), and
744 (G) in strains expressing oRNA1^{WT} or oRNA1^{mut} with or without heat shock. Data are mean with
745 standard deviation (N=4, biological replicates). Ratio paired t-test. **, p-value<0.05; **, p-value<0.01; ***,*
746 *p-value<0.001; ****, p-value<0.0001*.

747 **Figure 2: Signal from probes for antigenome is evident upon RNA denaturation**

748 (A) Representative smFISH images of uninfected (denatured) and infected animals (*jyIs8;rde-1*) with or
749 without dsRNA denaturation. *pals-5p::GFP* (green), oRNA1 genome (cyan), oRNA1 antigenome
750 (magenta), scale bar, 25μm. Column 4 shows an enlarged image of region boxed in column 3. White
751 arrowhead points to antigenome puncta. Pharynx signal (*) is from *mCherry*, a co-expression marker of
752 the integrated transgene (*jyIs8*). (N>3, biological replicates). Solid white lines outline animals, dashed
753 white lines outline infected intestinal cells. (B) Distribution of percent animals exhibiting antigenomic
754 signal (puncta) with or without denaturation (N=3, biological replicates). Total number of infected
755 animals is indicated. Representative images of OV-infected animals with or without denaturation using
756 either (C) antigenome or (D) genome smFISH probes only. oRNA1 genome (cyan), oRNA1 antigenome

757 (magenta), scale bar, 25μm. Solid white lines outline an animal, dashed white lines outline infected
758 intestinal cells, and white arrowhead points to antigenome puncta in column 3 (antigenome zoom of C).

759 **Figure 3: Probes to oRNA1 antigenome reveal perinuclear foci**

760 (A) Representative images of *jyIs8(wt)* or *jyIs8;rde-1(ne219)* animals infected with OV for 24 hours
761 along with corresponding line scan analysis (yellow arrow shows path of scan). Columns 1-3 depict
762 *pals-5p::GFP* (green), oRNA1 genome (cyan), antigenome (magenta), respectively. Merge zoom
763 (column 4) shows an enlarged image of the region boxed in columns 2 and 3 with signal from genome
764 and antigenome. Scale bar, 25μm. Infected cells are outlined with a white solid line and nuclei
765 (Hoechst) with a white dotted line. Pharynx signal (*) is from *mCherry,* a co-expression marker of the
766 integrated transgene (*jyIs8*). (B) Violin plot showing number of nuclei surrounded by genome smFISH
767 signal in indicated strains. Unpaired t-test with Welch's correction, ***; *p=0.0003* (C) Bar graph showing
768 percentage of infected animals exhibiting perinuclear localization of oRNA1 antigenome in infected cells
769 of *jyIs8(wt)* or *jyIs8;rde-1(ne219).* N=4, biological replicates. Total number of infected animals is
770 indicated in gray above each bar. (D-J) Representative images and line scans (yellow arrow shows
771 path of scan) of *jyIs8 (wt)* infected cells (white solid line) showing distribution pattern of oRNA1
772 antigenomic signal (magenta) in (D, E) perinuclear, (F, G) cytoplasmic, or (H, I) cytoplasmic foci, in
773 genome-containing infected cells, or (J) lumen (cyan, white solid line outlines infected animal). Dotted
774 lines indicate nuclei in G+AG (column 4) to enable visualization of nuclei in other columns. In (H),
775 showing cytoplasmic antigenome puncta, nucleus is unmarked since it is on a different z-plane.

776 **Figure 4: Perinuclear localization of oRNA1 antigenomic signal is partially dependent on**
777 **primary siRNA biogenesis but not secondary siRNA amplification**

778 (A) Representative images of OV-infected cells with distribution patterns of genome (G, cyan),
779 antigenome (AG, magenta) and nuclei (Hoechst, blue) at 24hpi. In column 1, infected worm is outlined
780 (solid white line) with total number (n) of infected animals visualized in all replicates. Scale bar, 25μm.
781 Columns 2, 3 & 4 show enlarged images of region boxed in column 1. Dotted lines indicate nuclei in
782 G+AG (column 4) to enable visualization of nuclei in other columns. (B) Violin plot showing number of
783 nuclei surrounded by genome smFISH signal in indicated strains. Kruskal-Wallis Multiple comparison

784 test, ***;p<0.01, ***; p<0.001, ****;p<0.0001.* (C) Quantification of percent infected animals exhibiting
785 perinuclear localization of oRNA1 antigenome at 24hpi in indicated strains. Data are mean with
786 standard deviation, N≥3, biological replicates. One-way ANOVA with Tukey's multiple comparison test.
787 **;p<0.05, ***;p<0.001.* (D) Representative northern blots showing viral siRNAs and U6 snRNAs
788 detected using antigenome smFISH probes or U6 DNA oligonucleotide probes (end-labeled with ^{32}P γ-
789 ATP); 3μg of total RNA isolated from indicated strains at 72hpi were used for each blot N=3. (E) As in
790 (D) using 2μg of total RNA from wildtype animals (72hpi) with or without terminator treatment. (N=3). %
791 value indicates the increase or decrease (indicated by arrows) in viral siRNA intensity after
792 normalization to U6 signal.

793 **Figure 5: Perinuclear localized oRNA1 antigenomic signal does not colocalize with known**
794 **antiviral RNAi factors**

795 (A) Schematic of antiviral RNAi pathway. Maximum Intensity Projection images as labeled for DCR-
796 1::3XFLAG::GFP, GFP::3XFLAG::RDE-1, DRH-3::GFP::3XFLAG, oRNA1 genome (cyan), oRNA1
797 antigenome (magenta) and merge in intestinal cells. Shown are localization patterns for uninfected
798 animals (B, C, D) or at 24hpi (E, G, H). Boxed region in (D) shows an enlarged image of perinuclear
799 localized DRH-3 in germline (inset). Columns 2,3 & 4 in E, G and H show infected cell (white solid line)
800 in region boxed in column 1. White arrowheads point to GFP puncta. Number in column 3 (n) indicate
801 the fraction of infected animals with GFP puncta in infected cells. (F) Line scan analysis of DCR-
802 1::3XFLAG::GFP infected cell showing distribution pattern of genome, antigenome and DCR-
803 1::3XFLAG::GFP. Yellow arrow shows path of scan. Over 40 infected animals were scored among 2
804 independent replicates for each strain. Scale bar, 25μm.

805 **Figure 6: oRdRP is present in spherical structures or dsRNA-associated puncta in OV infected**
806 **cells**

807 (A) Representative dot blot spotted with total RNA from uninfected and OV infected animals at 72hpi;
808 probed with J2 anti-dsRNA (J2) antibody. (N=3, biological replicates). (B) Representative images of
809 uninfected or infected (24hpi) *jyIs8* (wt) or *jyIs8;rde-1* dissected intestines (white solid outline). Infection
810 was signaled by expression of *pals-5p::GFP* (green) and also visualized were oRdRP (gray), dsRNA

811 (red), merge (oRdRP and dsRNA). Nuclei (as marked by Hoechst) outlined with white dotted line. Red
812 arrowheads, possible co-localization of oRdRP and dsRNA; white arrowheads, oRdRP spherical
813 structures; yellow arrowhead, oRdRP sphere near dsRNA puncta. Scale bar, 25μm; merge zoom,10μm.
814 N≥4 biological replicates with at least 5 animals per replicate for *jyIs8*; N=3 biological replicates with at
815 least 5 animals per replicate for *jyIs8;rde-1*. Signal from oRdRP in intestinal nuclei indicates non-
816 specific background staining. (C) Quantification of number of oRdRP spheres per infected animal in
817 indicated strains. Unpaired t-test with Welch's correction*; *, p=0.0424*. (D) Distribution of diameter of
818 each sphere measured from the infected animals. Unpaired t-test with Welch's correction*; *, p=0.0154*.
819 **Figure 7: Models for antigenomic perinuclear signal and oRdRP spheres.**
820 (A-C) Cartoons showing observed replication intermediates and their potential intersection with the
821 antiviral RNAi pathway. AVC factors are drawn to relative scale and adapted from Consalvo et. al.
822 (Consalvo *et al.*, 2024). A) In a wildtype animal, the perinuclear localized puncta could derive from OV
823 antigenome or viral siRNAs. (B) In AVC mutants, single mutants of DCR-1, DRH-1, or RDE-4, we
824 observed an increase in levels of viral RNAs and dsRNAs (Figures 1D, 1E, 6A and S1D-I), but the near
825 absence of viral siRNAs (Ashe *et al.*, 2013) leads to a reduction in the number of animals with
826 perinuclear localized antigenomic signal. (C) Deficiencies in RDE-1 do not exhibit changes in the
827 number of animals with perinuclear localized antigenomic puncta, despite these animals having an
828 increase in viral RNAs and dsRNAs. (D) In wildtype animals with efficient antiviral defense, oRdRP
829 spheres are abundantly formed as a part of viral clearance pathways. (E) In RDE-1 mutant animals,
830 due to impaired antiviral defense, fewer oRdRP spheres are observed.

831 **Figure 1**

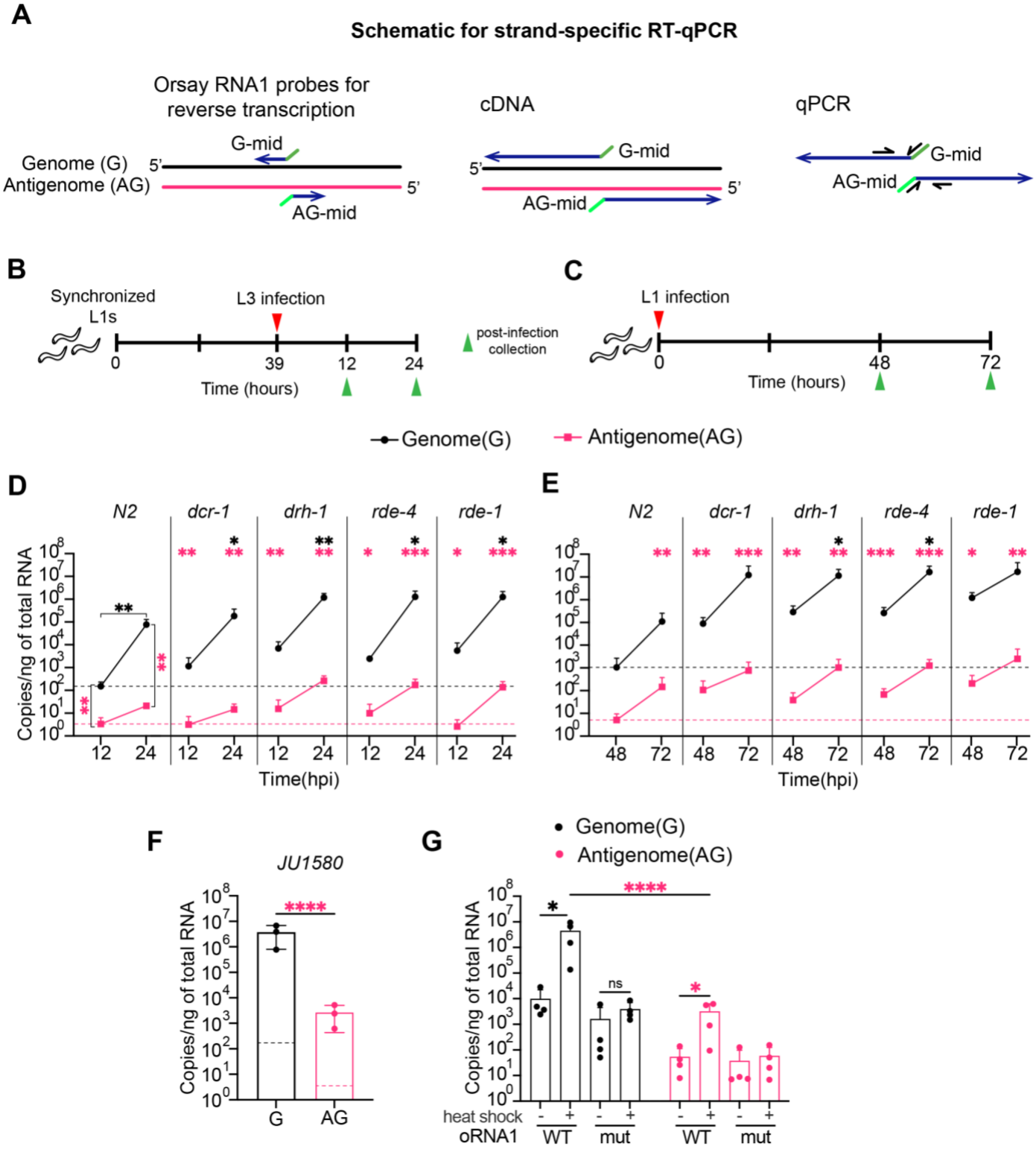

832

833 **Figure 2**

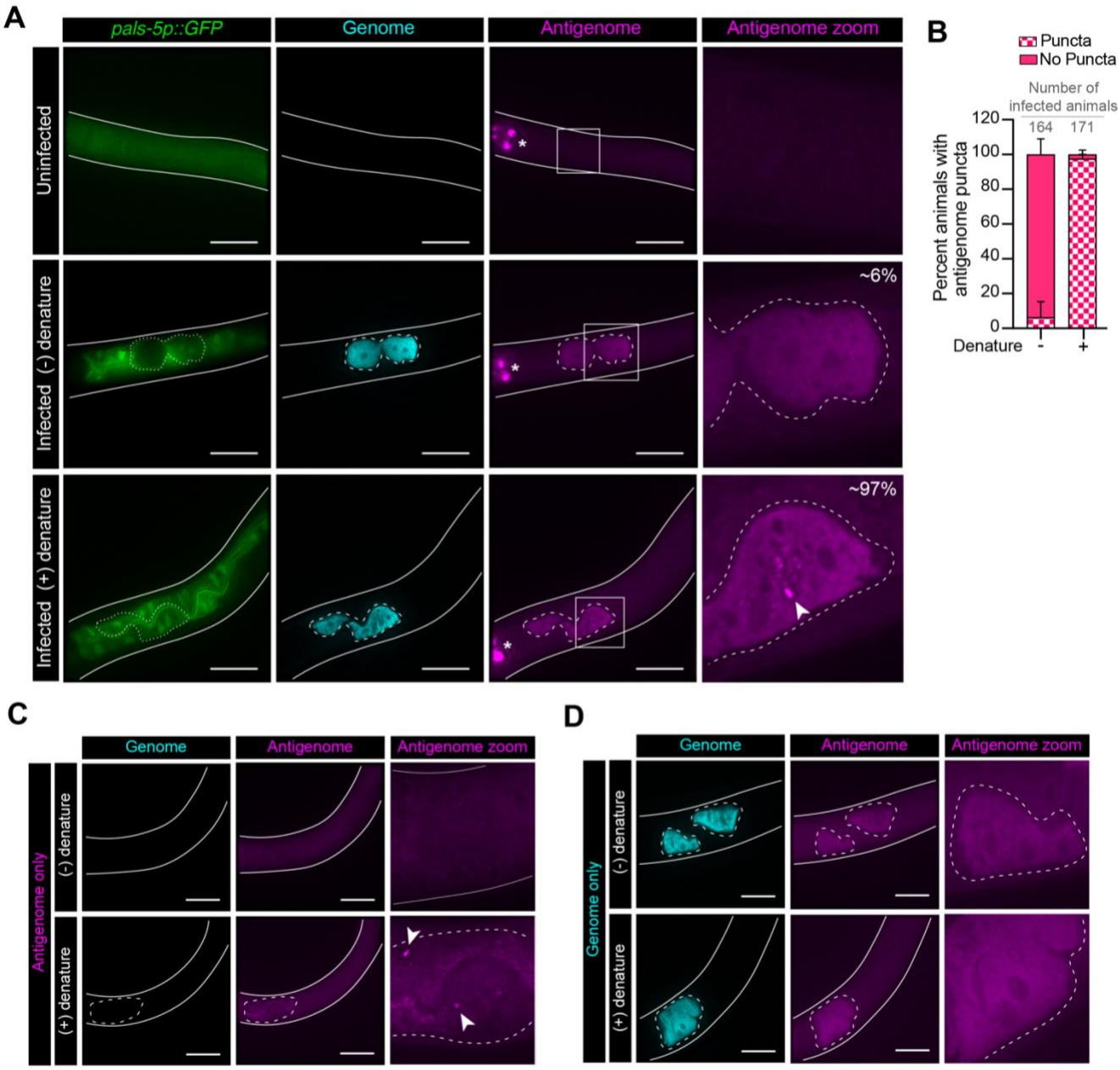

834

835 **Figure 3**

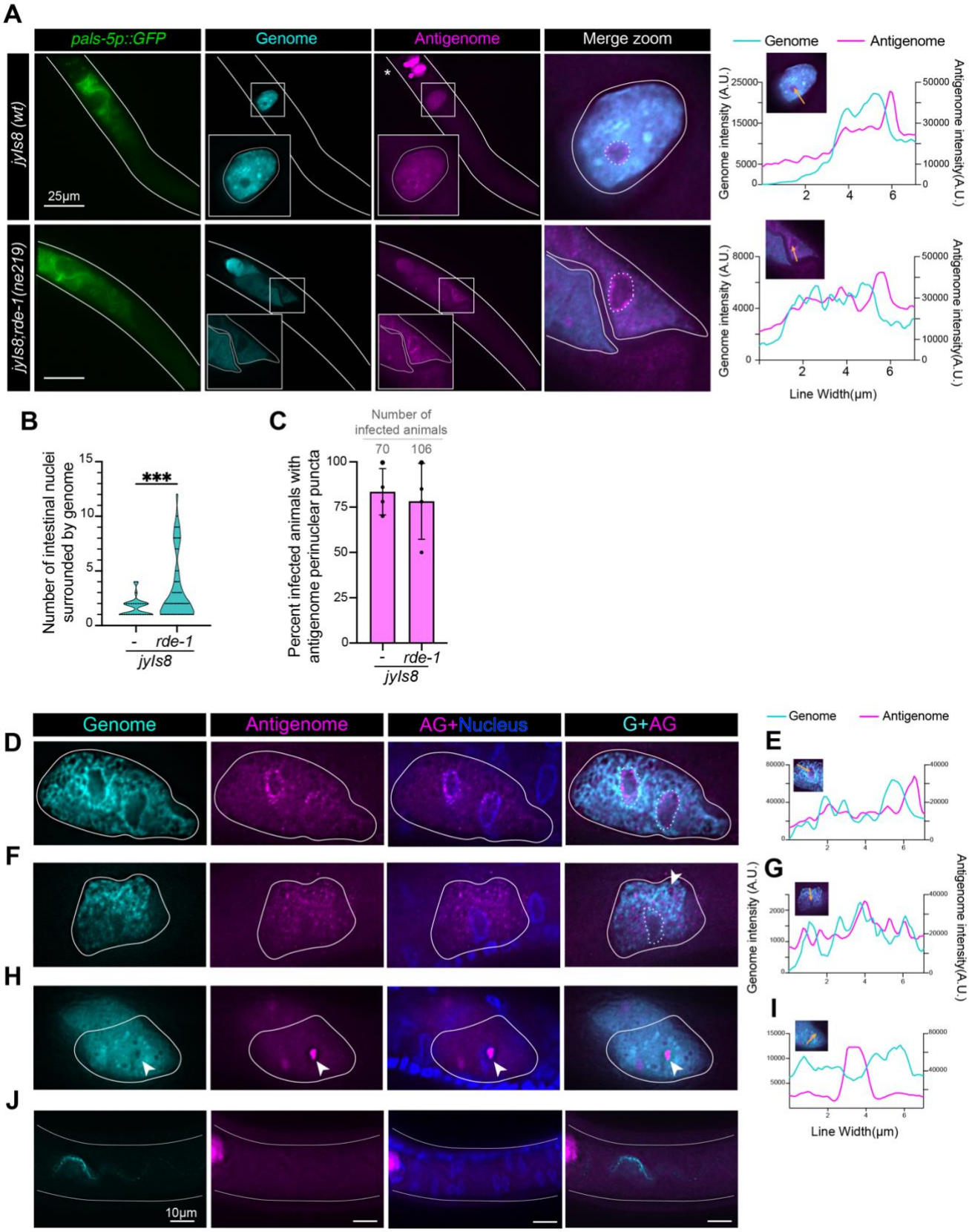

836

837 **Figure 4**

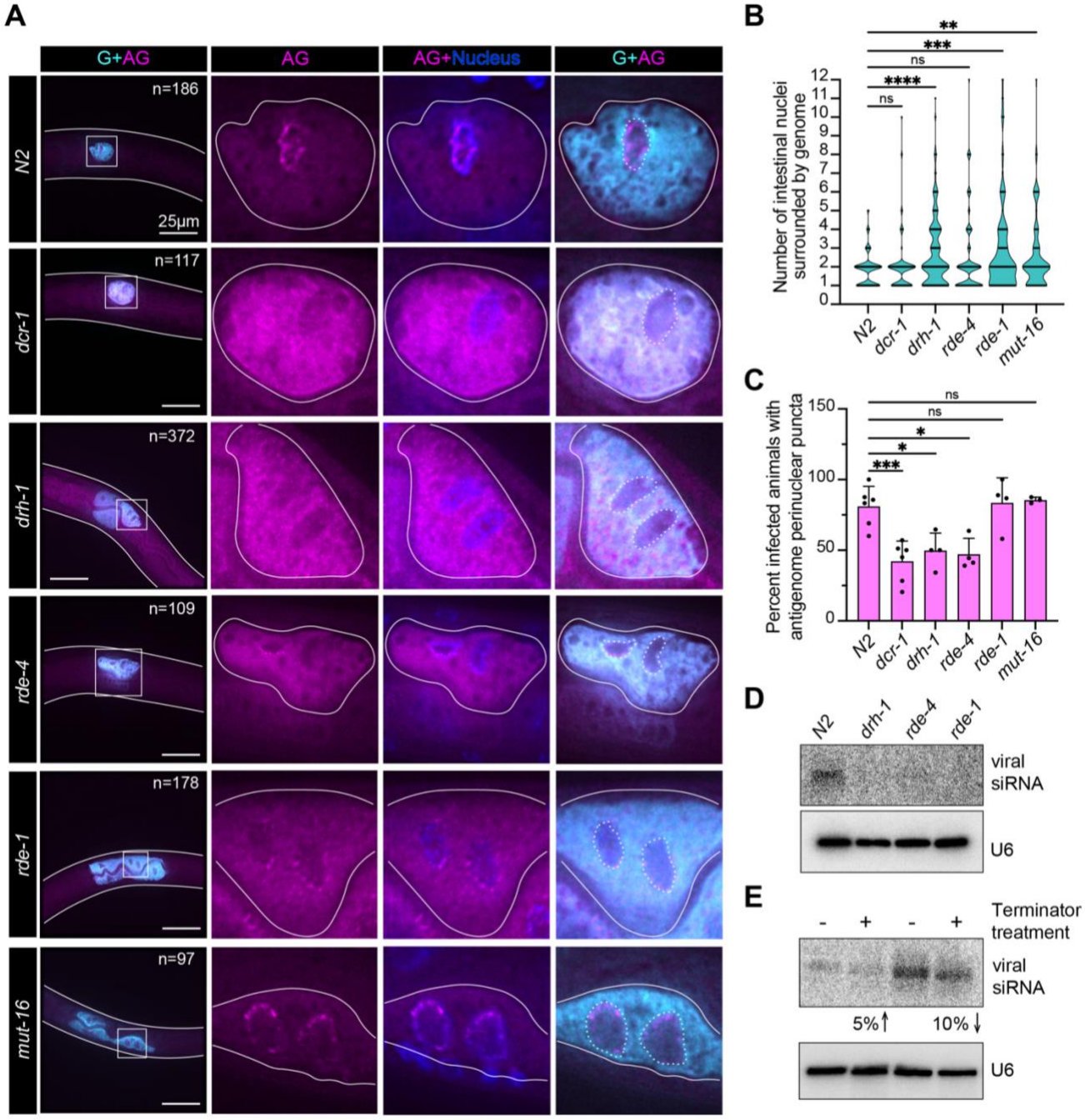

838

839 **Figure 5**

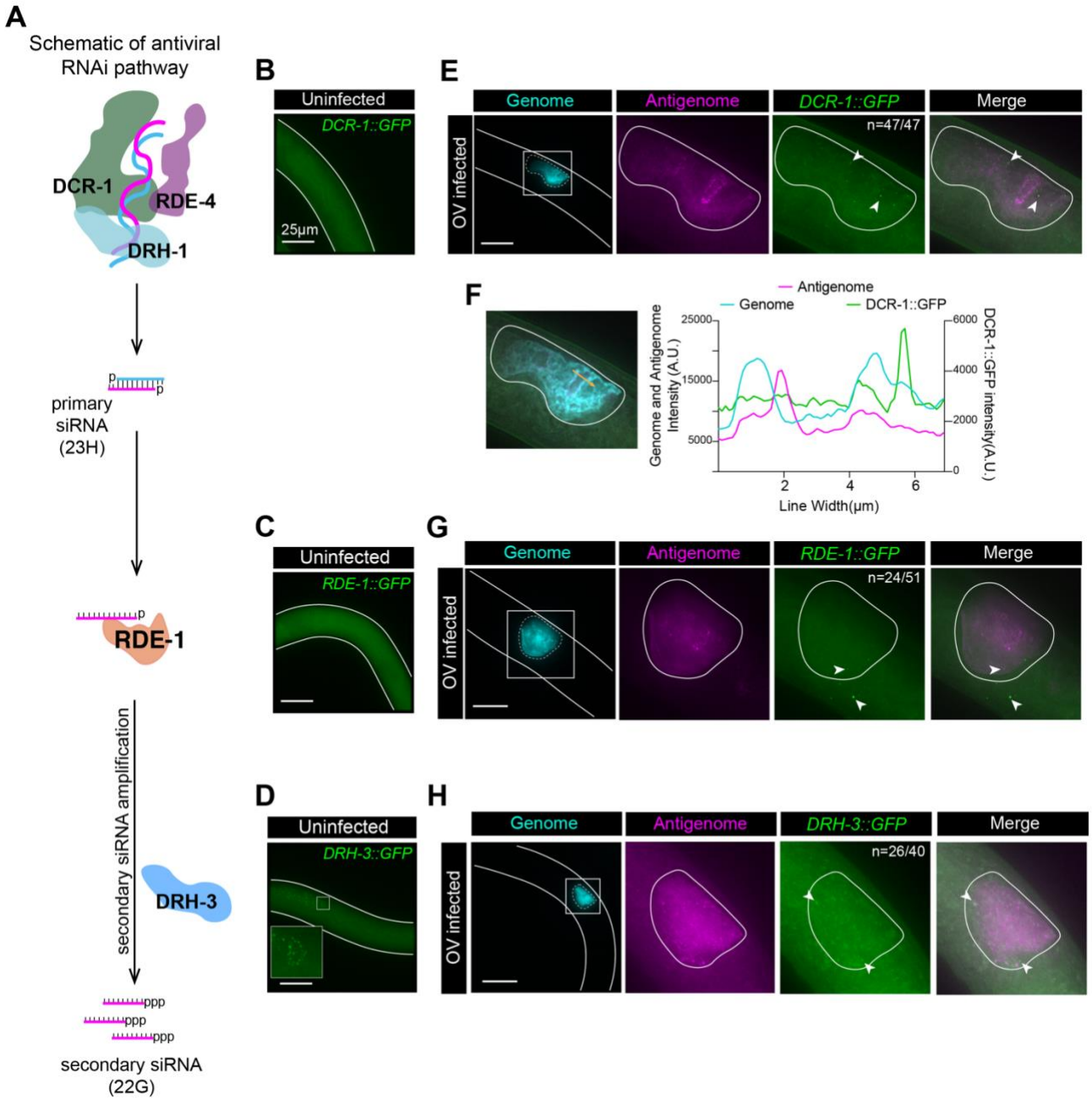

840

841 **Figure 6**

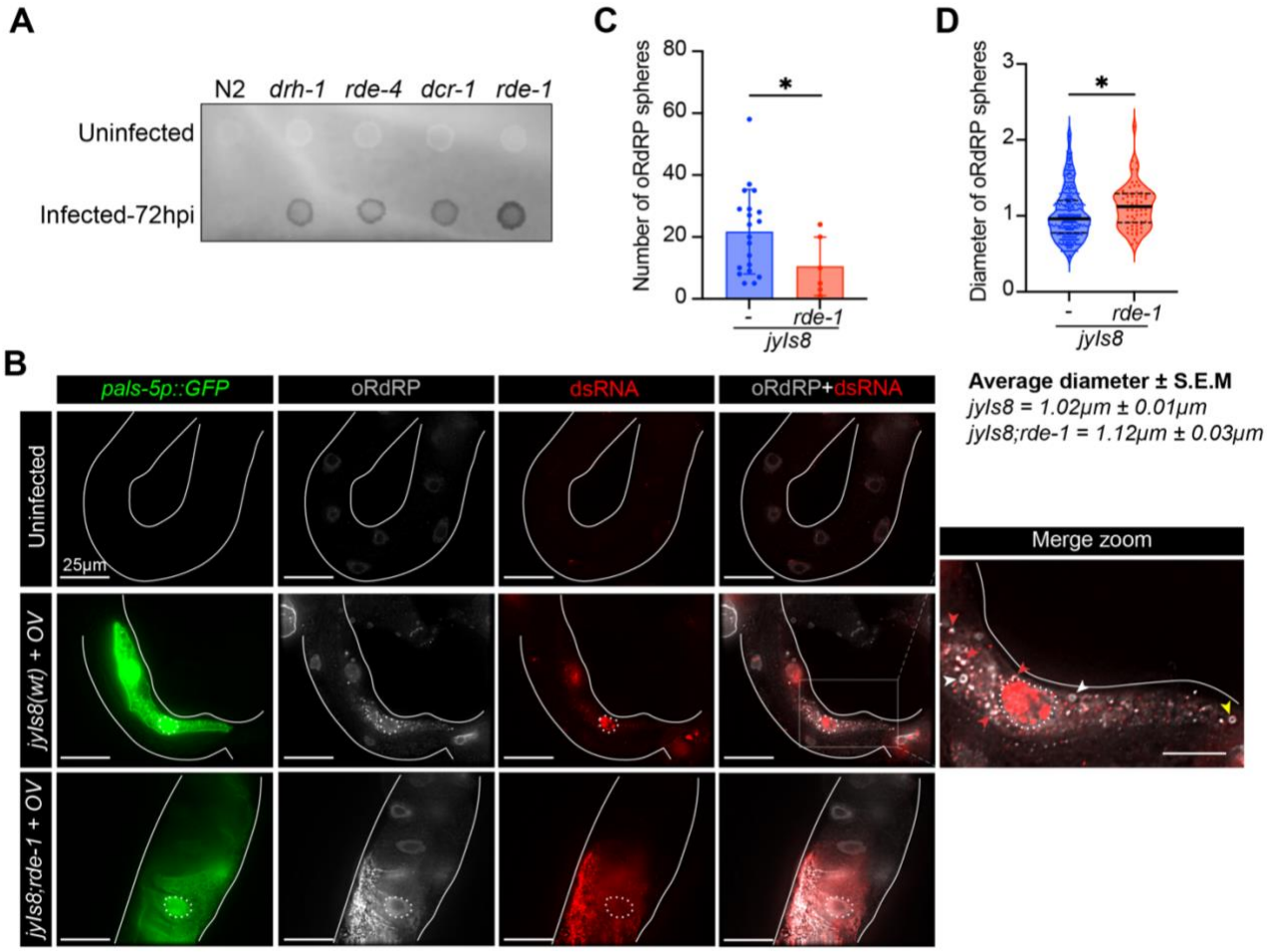

842

843 **Figure 7**

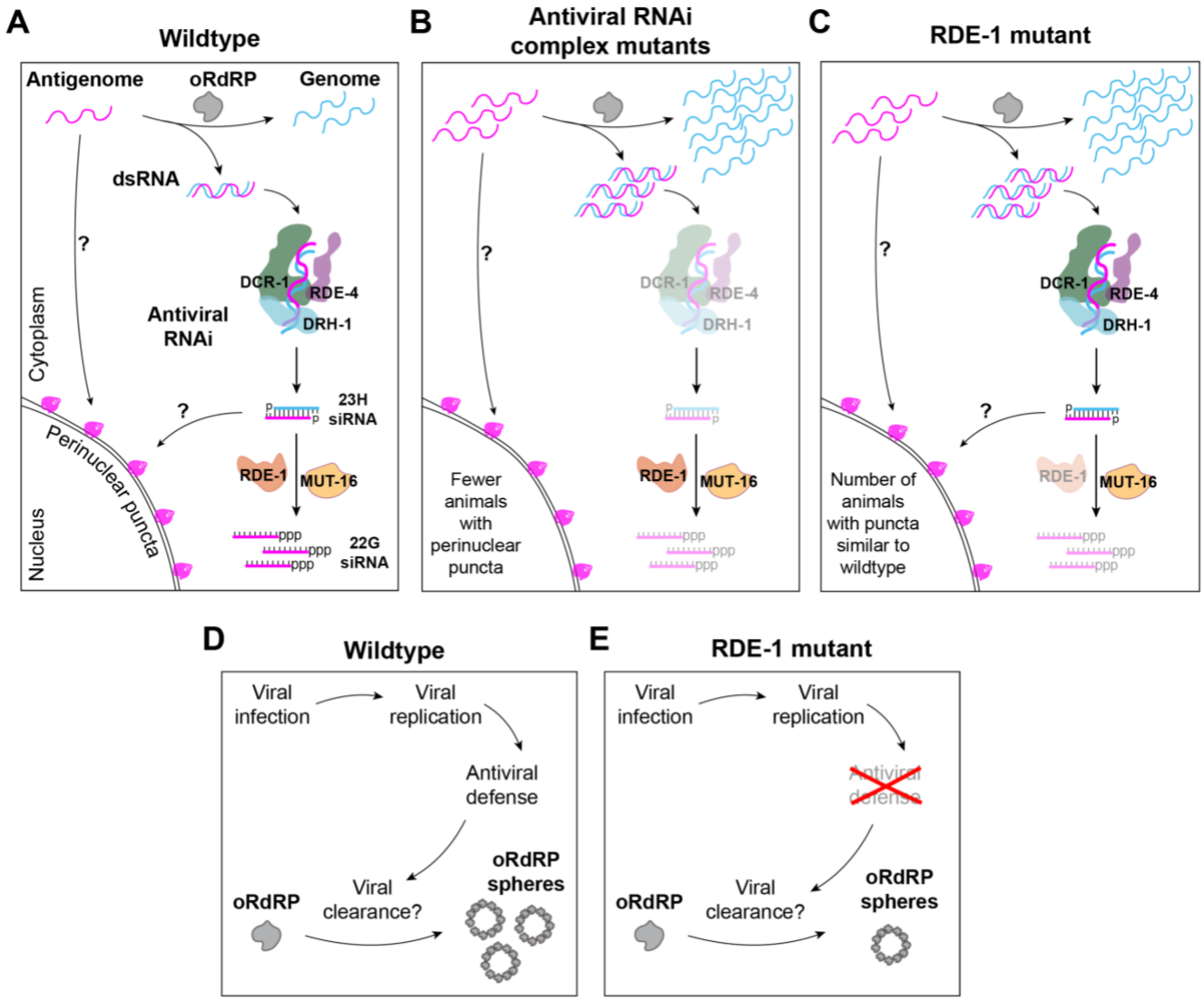

844